Available online at www.sciencedirect.com
ScienceDirect
Planetary and Space Science 57 (2009) 183–192
Planetary and Space Science
www.elsevier.com/locate/pss

Numerical simulations of asteroids modelled as gravitational aggregates with cohesion

D.C. Richardson[a,*], P. Michel[b], K.J. Walsh[b,a], K.W. Flynn[c,a]

[a]*Department of Astronomy, University of Maryland, College Park, MD 20742, USA*
[b]*University of Nice-Sophia Antipolis, UMR 6202 Cassiopée/CNRS, Côte d'Azur Observatory, B.P. 4229, 06304 Nice Cedex 4, France*
[c]*Dark Corner Software LLC, 11007 Lake Victoria Lane, Bowie, MD 20720, USA*

Received 15 January 2008; received in revised form 7 April 2008; accepted 22 April 2008
Available online 18 May 2008

Abstract

Evidence is mounting that asteroids larger than a few hundred metres in diameter are gravitational aggregates of smaller, cohesive pieces. For example, images of 25143 Itokawa show a boulder-strewn surface reminiscent of what might be expected following gravitational reaccumulation of material ejected from a catastrophic impact into a larger body. We have developed a new numerical approach to modelling gravitational aggregates that includes for the first time several prescriptions for variable material strength/cohesion while preserving the desirable features of fast and accurate computation from our prior methods. The new model can be used to construct non-idealized rubble piles made up of irregular, competent pieces, or to preserve shape and spin information of reaccumulated bodies in high-resolution simulations of asteroid family formation, by allowing fragments to stick on contact (and optionally bounce or cause further fragmentation, depending on user-selectable parameters). We detail the numerical method, which involves solving the rigid-body equations of motion and handling non-central/off-axis impacts, and present simulations of collisional and rotational disruption of asteroids as illustrative examples. This work is part of an ongoing effort to improve the realism and applicability of numerical simulations to the collisional and dynamical evolution of asteroids and other small solar system bodies.

Keywords: Asteroid structure; Asteroid dynamics; Asteroid satellites; Collisional physics; Impact processes

1. Introduction

The internal structure of asteroids is poorly understood, despite several spacecraft missions that have provided a wealth of *in-situ* data. There is growing indirect evidence that asteroids larger than a few hundred metres in diameter are aggregates of smaller cohesive pieces. We call such bodies "gravitational aggregates," because gravity is the principal force holding the body together (Richardson et al., 2002). A gravitational aggregate has little or no material cohesion between its components, so it can be disrupted by relatively weak tensile (outward-pointing) forces, such as those manifest in tidal encounters with planets (Richardson et al., 1998; Walsh and Richardson, 2006a, 2008) or generated by rotation arising from such forces as the "YORP" thermal effect (Rubincam, 2000; Vokrouhlický and Capek, 2002; Bottke et al., 2002, 2006). A "rubble pile" is a special case of gravitational aggregate that has moderate bulk porosity (i.e., a fair amount of internal void space, possibly due to jumbling of the body's components) and no cohesion between components.

The most compelling evidence so far that suggests asteroids may be gravitational aggregates (if not rubble piles), comes from images returned by the Hayabusa spacecraft of asteroid 25143 Itokawa (Fujiwara et al., 2006). These images show an irregular ~500 m long body with a boulder-strewn surface, as might be expected from reaccumulation following catastrophic disruption of a larger parent asteroid (Michel et al., 2001). The inferred low bulk densities of many primitive asteroids, obtained either by direct spacecraft measurement (e.g., Yeomans et al., 1997), or inferred from the orbits of satellites (e.g., Merline et al., 1999), are also suggestive of possible

*Corresponding author. Tel.: +1 301 405 8786; fax: +1 301 314 9067.
E-mail address: dcr@astro.umd.edu (D.C. Richardson).

0032-0633/$ - see front matter © 2008 Elsevier Ltd. All rights reserved.
doi:10.1016/j.pss.2008.04.015

jumbled interiors: bulk porosities of 40–60% are required if such bodies are the parents of chondritic material on Earth. Simulations of catastrophic main-belt impacts followed by gravitational reaccumulation of fragments are a good match for present-day asteroid families (Michel et al., 2001, 2002, 2003, 2004a, b; Durda et al., 2007), and can lead to binary formation (Durda et al., 2004; also see Richardson and Walsh, 2006). Indeed, after their long history of sub-catastrophic impacts, surviving present-day asteroids of diameter $\gtrsim$100 m likely have fractured or rubblized interiors, which may explain how asteroids such as 253 Mathilde endured giant-crater-forming impacts (the jumbled interior strongly damps propagation of the impact shock energy: Asphaug et al., 1998; also see Asphaug and Melosh, 1993 and Veverka et al., 1997; an alternative explanation is that the impact energy went into crushing microporous surface material: Housen et al., 1999; Housen and Holsapple, 2003).

Pravec and Harris (2000) and also Pravec et al. (2002, 2005) noted from lightcurve data that most near-Earth asteroids (NEAs) with diameters $\gtrsim$150 m spin below the breakup limit for cohesionless objects (for an assumed typical bulk density), and moreover that there is a large concentration of bodies just inside that limit, suggesting that most objects can spin up to their breakup point, but not beyond, possibly because most are cohesionless or nearly so. However, Holsapple (2007) points out that even bodies with some cohesion, if they are large enough that their self-gravity makes the contribution of their cohesion irrelevant, will break up near the cohesionless spin limit, so the existence of a spin barrier does not require these bodies to be cohesionless *per se*; nonetheless, such bodies are still subject to rotational disruption. Most fast rotators (period $\lesssim$2 h) are small bodies $\lesssim$100 m for which material strength is expected to dominate over gravitational cohesion (e.g., Love and Ahrens, 1996; Asphaug et al., 1998). However, Holsapple (2007) also suggests that sustaining such fast rotation only needs a very small but non-zero cohesion, so even these small bodies may have some aggregate structures.

Although not an asteroid, the breakup and subsequent impact into Jupiter of Comet D/Shoemaker-Levy 9 (SL9) spurred the idea that small solar system bodies may be fragile in general. Asphaug and Benz (1994) showed that the SL9 breakup into the so-called "string of pearls" was consistent with tidal disruption of a gravitational aggregate followed by gravitational reaccumulation of the fragments. This is a very generic result that depends only on gravity (Richardson et al., 1998; Walsh et al., 2003; Walsh and Richardson, 2006a, 2008). The presence of crater chains on the jovian moons (Schenk et al., 1996) and one or two on Earth's moon (Bottke et al., 1997) indicate that this process has occurred repeatedly to comets and possibly even asteroids over the lifetime of the solar system. Other evidence for small solar system bodies being gravitational aggregates includes the unusual shapes of certain asteroids derived from delay-Doppler radar imaging, indicative of tidal distortion (Ostro et al., 1995; Bottke et al., 1999), the large fraction of doublet craters on the terrestrial planets, which can be explained by tidal fission of rubble-pile asteroids (Bottke and Melosh, 1996a, b), the mysterious disintegration of Comet C/1999 S4 (LINEAR) (cf. Farnham et al., 2001) and others, and the Galileo spacecraft measurement of the surprisingly low density of Jupiter's moon Amalthea (Anderson et al., 2002).

The notion that small solar system bodies are fragile motivates theoretical studies into the origin and evolution of such bodies. We have developed computer code, an extension of the *N*-body package `pkdgrav` (Stadel, 2001), for performing numerical simulations of the collisional and gravitational dynamics of aggregates, with or without cohesion. The code uses a hierarchical tree algorithm to reduce the cost of computing interparticle forces, and parallel structure to balance the work among multiple processors, so that simulations of tens of thousands to even millions of strongly interacting/colliding particles are feasible. Earlier simulations of gravitational aggregates typically consisted of idealized rubble piles made up of equal-size solid spheres (Richardson et al., 2005). Such code has been used to follow the fragments generated by the disruption of a large asteroid during the subsequent ejection and reaccumulation phase (Michel et al., 2001, 2002, 2003, 2004a, b). But in these simulations, fragment shapes were limited to perfect spheres, and when fragments collided with each other, they merged into a single sphere (or bounced off each other, depending on their relative impact speeds). So, the determination of the final shape of fragments could not be addressed. Recent work on other codes has led to less idealized models featuring, for example, ellipsoids instead of spheres (Roig et al., 2003) or more complex polyhedral shapes (Korycansky and Asphaug, 2006), but these are computationally much more expensive and therefore limited to far fewer particles. Recently we have developed a numerical method in which spheres can be bonded together into coherent units that interact both gravitationally and collisionally. We call the units "bonded aggregates" to distinguish them from rubble piles; if the bonds are weak, the bodies are still gravitational aggregates. Since the components of each bonded aggregate are spheres, collision detection is simplified, and the full tool set of the numerical code for reducing the cost of point-particle force calculations can still be exploited. In Section 2 we describe the numerical method in detail. In Section 3 we present preliminary simulations using the new method. In Section 4 we discuss future applications and development.

2. Method

We use `pkdgrav`, a numerical gravity solver, first developed for cosmological modelling at the University of Washington (Stadel, 2001). The code was adapted to

treat hard-sphere collisions for planetesimal modelling (Richardson et al., 2000). The main technical features of the code include a hierarchical tree algorithm for reducing the computational cost of interparticle force calculations and a complete parallel implementation for balancing work across an arbitrary number of processors. These features place `pkdgrav` among only a handful of fast codes available to the astronomy/planetary science community for modelling complex systems of gravitationally and collisionally interacting particles. Many aspects of the code, including the ability to model semi-rigid bodies (bonded aggregates), are, as far as we know, unique to `pkdgrav`.

2.1. Equations of motion

Fundamentally, `pkdgrav` solves Newton's equations of motion for self-gravitating point particles,

$$\ddot{\mathbf{r}}_i = -\sum_{j\neq i} \frac{Gm_j(\mathbf{r}_i-\mathbf{r}_j)}{|\mathbf{r}_i-\mathbf{r}_j|^3}, \tag{1}$$

where $\mathbf{r}$ denotes position (in three spatial dimensions), m is mass, G is the gravitational constant, $i,j\in[1,N]$ are indices, N is the number of particles, and the derivatives are with respect to time. In the absence of time-saving measures such as the treecode, computation of interparticle forces scales as $\frac{1}{2}N(N-1)$ (the $\frac{1}{2}$ comes from Newton's law of reciprocal actions), or $\mathcal{O}(N^2)$ for $N\gg 1$. With the treecode, the potentials due to distant groups of particles are approximated by multipole expansions about the group centers of mass, resulting in computation times that scale as $\mathcal{O}(N\log N)$, but that gives rise to small force errors (cf. Barnes and Hut, 1986). The errors (usually $\ll 1\%$ in our simulations) are controlled by a single parameter that determines how small and distant a group of particles must be to use the approximation. Typical implementations expand the potentials to quadrupole order; `pkdgrav` expands to hexadecapole order.

The $6N$ coupled ordinary differential equations of Eq. (1) are solved using a second-order "leapfrog" integrator:

$$\begin{aligned}
\dot{\mathbf{r}}_{i,n+1/2} &= \dot{\mathbf{r}}_{i,n} + (h/2)\ddot{\mathbf{r}}_{i,n} \quad \text{"kick"},\\
\mathbf{r}_{i,n+1} &= \mathbf{r}_{i,n} + h\dot{\mathbf{r}}_{i,n+1/2} \quad \text{"drift"},\\
\dot{\mathbf{r}}_{i,n+1} &= \dot{\mathbf{r}}_{i,n+1/2} + (h/2)\ddot{\mathbf{r}}_{i,n+1} \quad \text{"kick"},
\end{aligned} \tag{2}$$

where h is the (constant) timestep that takes the system from step n to step $n+1$. Each stage in the kick–drift–kick sequence is performed for all particles i. The timestep h is chosen to ensure adequate sampling of the shortest dynamical time in the system, which is typically $\sim 1/\sqrt{G\rho}$, where ρ is the characteristic mass density of a particle. The principal advantage of the leapfrog method, which as shown "kicks" the particle velocities while holding the positions constant, then "drifts" the particle positions while holding the velocities constant, is that it is symplectic, meaning it has good conservation properties for sufficiently small, constant h (see Saha and Tremaine, 1992 for details; note however, that the tree is not strictly momentum conserving, and collisions remove energy from the system). Another advantage is that it makes collision detection particularly simple (Section 2.2). In the leapfrog scheme, the accelerations $\ddot{\mathbf{r}}_i$ are computed using the treecode after each drift (and once at the very start of the simulation), before the next kick.

2.2. Collision handling

For modeling collisions between particles, each particle is treated as a rigid sphere of given radius. Since particle positions change only during the drift step, and the change is linear in time, collisions between particles can be predicted by solving a quadratic equation for the time of surface contact between any two approaching spheres (Richardson et al., 2000; Appendix A). This is an approximation since in reality the particles generally do not move through the intervening space in straight lines; errors arising from this simplification can be reduced by shortening the timestep (usually the timestep is chosen to be a small fraction of the dominant dynamical timescale of the system, meaning the trajectories are nearly linear anyway over the timestep). To reduce the cost of the collision search, a variant of the `pkdgrav` tree algorithm is used to find the N_n closest neighbours of each particle (the method scales as $N_n\log N$). Typically $N_n\sim 16$, which is sufficient to find all possible colliders in a close-packed configuration of equal-size particles, and allows for the possibility of detecting collisions with more distant neighbours approaching at faster relative speeds. For collisional simulations involving a range of particle sizes, or featuring high particle speeds well outside of dynamical equilibrium, N_n needs to be increased.

A collision search is performed for all particles at the beginning of the drift step, and any potential collisions found are processed in time order. Once a collision is detected, the outcome is determined based on user-defined parameters that include the amount of dissipation (restitution and surface friction) and whether particles stick or bounce on contact. Particles that stick result in the formation of a bonded aggregate. For bouncing, billiard-ball restitution equations are used (including spin, if there is surface friction; cf. Richardson, 1994). After a collision, the particles involved (and any particles in the system that were identified as possibly colliding with either of the colliders later in the drift interval) are subjected to a new potential collider search. In this way, all collisions are detected and processed in the correct time order, even if a given particle suffers more than one collision in a drift interval (which is often the case for close-packed configurations). Once all collisions have been handled, the final end-of-drift particle positions are assigned and the interparticle gravity is computed.

2.3. Bonded aggregates

A new feature of `pkdgrav` is the ability to model the behaviour of bonded aggregates of spheres that are constrained to move as a single unit. Such aggregates can already exist at the start of a simulation, or gradually form during a simulation if particle sticking is enabled. In the code, each aggregate is treated as a "pseudo-particle" with center-of-mass position and velocity computed from its constituent particles (which are otherwise treated as independent bodies). Each aggregate has a unique identifier that is used when collecting information from its constituent particles (which may be distributed over more than one processor). The mass centers of bonded aggregates, i.e., the pseudo-particles, obey the usual equations of motion, with the center-of-mass acceleration of each aggregate computed as the mass-weighted average of the accelerations of their constituent particles before each kick. In addition, however, the rigid-body Euler equations must be solved for the rotation (cf. Richardson, 1995),

$$I_1\dot{\omega}_1 - \omega_2\omega_3(I_2 - I_3) = N_1,$$

$$I_2\dot{\omega}_2 - \omega_3\omega_1(I_3 - I_1) = N_2,$$

$$I_3\dot{\omega}_3 - \omega_1\omega_2(I_1 - I_2) = N_3, \tag{3}$$

(where I_k are the principal moments of inertia of the body, ω_k are the spin components in the body frame, and N_k are the net torque components in the body frame), and for the principal axis orientations,

$$\dot{\hat{\mathbf{p}}}_1 = \omega_3\hat{\mathbf{p}}_2 - \omega_2\hat{\mathbf{p}}_3,$$

$$\dot{\hat{\mathbf{p}}}_2 = \omega_1\hat{\mathbf{p}}_3 - \omega_3\hat{\mathbf{p}}_1,$$

$$\dot{\hat{\mathbf{p}}}_3 = \omega_2\hat{\mathbf{p}}_1 - \omega_1\hat{\mathbf{p}}_2, \tag{4}$$

(where $\hat{\mathbf{p}}_k$ denote the principal axes). This set of 12 equations for each aggregate is solved using a fifth-order time-adaptive Runge–Kutta integrator during the drift step (the equations are not easily adapted to the leapfrog integrator). The torque is given by

$$\mathbf{N} = \mathbf{\Lambda}^{\mathrm{T}}\left[\sum_{i\in a} m_i(\mathbf{r}_i - \mathbf{r}_a)\times(\ddot{\mathbf{r}}_i - \ddot{\mathbf{r}}_a)\right], \tag{5}$$

where the summation is over all particles belonging to the aggregate, $\mathbf{r}_a$ is the aggregate's center-of-mass position, and $\mathbf{\Lambda} \equiv (\hat{\mathbf{p}}_1|\hat{\mathbf{p}}_2|\hat{\mathbf{p}}_3)$ is a matrix—whose columns are the principal axes of the aggregate—that transforms vector quantities from the body frame to the space frame (so the transpose does the opposite). Computing the torque is $\mathcal{O}(N)$, so it does not add significantly to the overall simulation cost. The principal moments and axes are computed by diagonalizing the inertia tensor of each aggregate (cf. Richardson, 1995), which is done whenever a particle is added to or removed from the aggregate.

2.4. Modified collision handling

The presence of bonded aggregates complicates collision prediction and resolution. Although particles within a bonded aggregate by definition do not collide with one another (since they are constrained to have no relative motion, a fact that can greatly speed up collision searches), the rotational motion of these bodies means that the time of collision with an external particle (perhaps itself part of a bonded aggregate) cannot be solved exactly. Instead, the quadratic time-of-collision equation is modified slightly to account for the rotational motion expanded to second order using a Taylor series (see Appendix A). This is a necessary approximation, and in any case the orientation of the aggregate(s) is advanced to the estimated time of collision using the Runge–Kutta integrator, so the precise circumstances of the impact may be slightly in error relative to the prediction. In the event of a missed collision, special overlap handling methods (not discussed here) quickly correct the problem. Tests show that numerical artifacts are negligible and that the expected physical behaviour occurs when bonded aggregates collide (for example, bouncing cubes settle to a minimum energy configuration with faces touching and without relative motion; see Fig. 1).

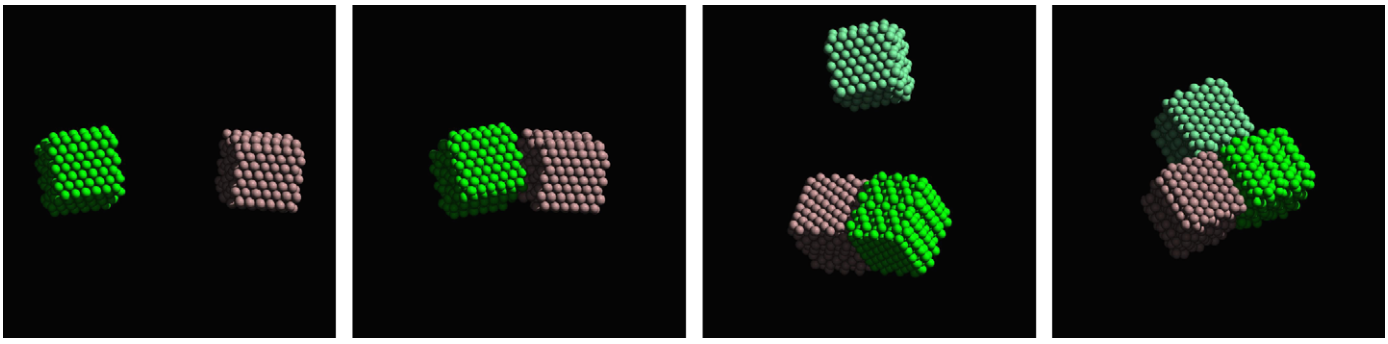

Fig. 1. Snapshots of three colliding rigid cubes made up of identical spheres. The cubes experience torques via mutual gravity and collisions. The collisions are dissipative. In this example the cubes quickly achieve a minimum energy state where they present only flat faces to each other. There is net (non-zero) total angular momentum in this system.

There are three supported collision outcomes for bonded aggregates: sticking on contact (to grow the aggregate); bouncing (computed for these generally non-central impacts using the method of generalized coefficients—cf. Brach, 1998; Richardson, 1995; for completeness, a summary of the pertinent equations is given in Appendix B); and fragmentation (wherein the particles involved become detached from their respective aggregates and proceed to bounce as rigid spheres, possibly releasing more particles). Currently the user can specify which of these outcomes are allowed, and the circumstances under which each is invoked (generally given as an impact speed threshold relative to the surface gravitational escape speed). Angular momentum is conserved in each case, while energy may be dissipated depending on the adopted coefficient of restitution. The angular momentum of an aggregate relative to its center of mass in the space frame can be expressed either as $\mathbf{h} = \mathbf{I}\boldsymbol{\omega}$, where $\mathbf{I}$ is the aggregate's inertia tensor and $\boldsymbol{\omega}$ is its spin vector, or by

$$\mathbf{h} = \sum_{i \in a} \left[m_i(\mathbf{r}_i - \mathbf{r}_a) \times (\dot{\mathbf{r}}_i - \dot{\mathbf{r}}_a) + \frac{2}{5} m_i s_i^2 \boldsymbol{\omega}_i \right], \tag{6}$$

where s_i and $\boldsymbol{\omega}_i$ are the radius and spin vector, respectively, of each constituent spherical particle (for particles fixed in an aggregate, $\boldsymbol{\omega}_i$ is equal to the spin vector $\boldsymbol{\omega}$ of the aggregate as a whole). If an aggregate gains or loses mass, Eq. (6) is used to determine its angular momentum after the mass change. By conservation of momentum, the result is equal to $\mathbf{I}\boldsymbol{\omega}$, yielding the new spin vector $\boldsymbol{\omega}$, and hence the new $\boldsymbol{\omega}_i$ of each constituent particle, and the new constrained velocities $\dot{\mathbf{r}}_i = \boldsymbol{\omega} \times (\mathbf{r}_i - \mathbf{r}_a) + \dot{\mathbf{r}}_a$. In the case of mass loss, the liberated particle(s) carry away some angular momentum, in accordance with conservation laws.

2.5. Strength models

The fragmentation outcome discussed above is a simple model of fracture formation at (and propagation from) the point of impact. We have also implemented some simple strength models in an ongoing effort to mimic the stress response of real materials to rotation and tidal forces (see Holsapple, 2007). These models are still under development, so only brief discussions are given here.

2.5.1. Rigid failure

In this model, bonded aggregates are given a size-dependent strength ($S \propto R^{\alpha}$, where R is the aggregate effective radius) in either the normal (tensile) or tangential (shear) directions, or both. The aggregate experiences no strain as the stress increases: it remains perfectly rigid until the strength is exceeded. The failure test is performed at each step immediately following the gravity calculation: each bonded aggregate is checked in turn to see if any constituent particles are experiencing a differential acceleration relative to the aggregate center of mass that exceeds the user-supplied strength law, in either the normal (for tensile stress) or tangential (for shear stress) direction. This stress can arise from gravitational tidal effects due to close encounters with other bodies in the system, fast rotation, or both, and includes the effect of self-compression since all interparticle forces are computed explicitly, even those arising between particles within an aggregate. Particles experiencing excessive stress are liberated from the aggregate and become free particles in the system. Free particles that stick to an aggregate (if that outcome is allowed) immediately inherit the full strength of the aggregate. We do not keep track of weak bonds, or cracks, etc. For these calculations, the strength (in units of pressure) is converted to a maximum acceleration by multiplying by the cross-sectional area[1] and dividing by the mass of the particle under consideration. Note that since we do not track fractures or cracks, this failure model is only a crude approximation to the behaviour of real cohesive materials (which generally fail at their weakest point, for a sufficiently slowly increasing stress).

2.5.2. Elastic failure

Since there is no strain in the rigid failure model, it has an "all-or-nothing" response to impulsive stress, such as a tidal encounter, and the liberated particles generally escape to infinity (also see Fig. 3 in Section 3). This is not conducive to, for example, binary formation, which motivates a second model in which the aggregate can experience some strain (increasing separation between constituent particles) before failure. The inverse of the ratio of the strain response to the applied stress is Young's modulus. For this model we do not use the rigid aggregate code (because the particles must be free to move) but instead add a restoring force between particles that is proportional to the strain (and hence Young's modulus times the stress), up to a maximum stress. The user supplies Young's modulus and the maximum allowed stress. If the stress limit is exceeded (relative to all neighbouring particles), the particle is permanently liberated, so returning particles do not regain their cohesion. As with the rigid failure model, the restoring force is expressed as an acceleration by multiplying the stress by the particle cross-sectional area divided by its mass. Internally, liberated particles are flagged so that they no longer feel a restoring force, even if they come back in contact with the remnant aggregate. The computation of strains and restoring forces is done each step after the interparticle gravity calculation and uses the same neighbour search tree as for collision detection. For simplicity, particles are assumed to experience no relative stress if they are nearly in contact, so that a close-packed rubble pile starts in an almost stress-free state. As the particles become displaced from one another, the stress builds. A better approach would be to measure displacement from a fixed initial

[1] Strictly speaking, because our aggregates have voids, the effective area could be reduced by a porosity factor less than unity, but since the exact value is uncertain, we omit this detail from our treatment for now.

lattice; this is a future project that will require considerable code development to be of general use.

3. Simulations

3.1. Gravitational reaccumulation

The principal motivation for adding bonded aggregates to `pkdgrav` is to address the limitations of the reaccumulation model used in asteroid family/satellite formation simulations (e.g., Michel et al., 2001; Durda et al., 2004), namely that reaccumulating particles are merged into single spheres if they impact at slow speed, thus losing important shape and spin information. In the case of satellite formation in particular, retaining some shape/spin information is needed in order to provide a more realistic gravity field in proximity to the largest remnant, which is the most important factor in dictating the stability of any satellites. Although more computationally expensive than the simple merging model, bonded aggregates permit many more particles to be used than simulations that do not allow any merging or sticking at all, because the number of collisions occurring per timestep in the largest remnant would be prohibitively large in the latter case.

Fig. 2 shows a snapshot of the largest reaccumulated remnant following a high-speed disruptive impact into an asteroid (in the manner of Michel et al., 2001). Here we used the bonded aggregate model with collisional and rotational/tidal fragmentation enabled (using the rigid failure approach). The bulk of the body formed from the material that experienced the least amount of acceleration after the impact, but the rest of it consists mostly of large fragments that reaccumulated on their own and then fell back onto the largest remnant (this is made evident by the colour scheme in the figure: aggregates that form independently retain a unique colour, even if they subsequently bond with another aggregate). In this model the sticking criterion was set to 10% of the relative escape speed, so most clumps and single particles bounce (with dissipation) for a while on the surface before sticking. This leads to fairly efficient packing, as seen in this example. It is interesting to compare this outcome with images of Itokawa: similarities in overall structure and the presence of large surface components are striking. However, it must be emphasized that we are using a very simple prescription for complicated mechanical processes. Much work remains to determine the validity and applicability of these models. Encouragingly, the size and velocity distribution of the reaccumulated fragments in these tests match well with the original models that used the simple spherical merging model (which in turn match well with observed asteroid families), indicating the robustness of the conclusion that gravitational reaccumulation plays a key role in asteroid family formation (Michel et al., in preparation). We have begun to explore the effects of stepsize, stick/bounce threshold, overlap handling method, strength model, etc. on the outcome. So far the end results largely differ only in the details, e.g., the largest remnant mass remains fairly consistent, but the distribution and arrangement of the reaccumulated fragments vary. This is to be expected given the many degrees of freedom in the problem.

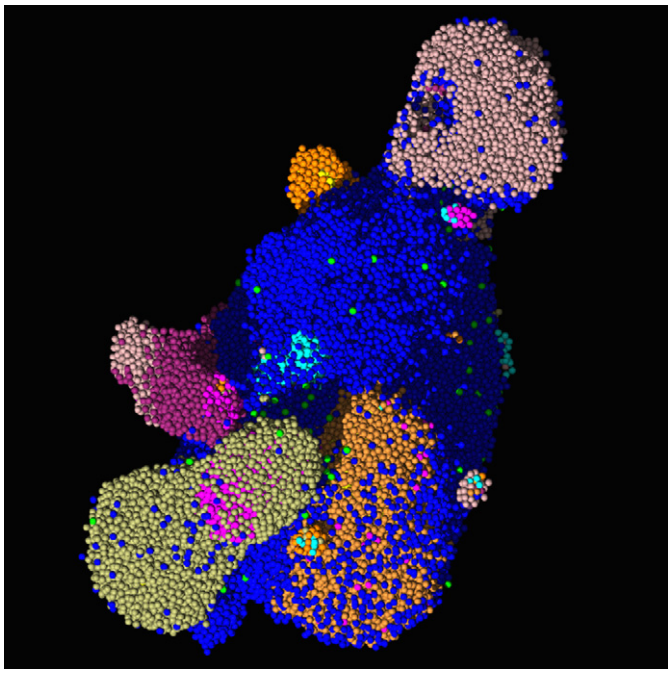

Fig. 2. Snapshot of the largest reaccumulated remnant approximately 11 days after the disruption of a 25 km diameter pre-fragmented basalt asteroid by a 2.4 km radius projectile travelling at $5\,\mathrm{km\,s^{-1}}$ at an impact angle of 45°, corresponding to a specific impact energy of $1.13\times10^{8}\,\mathrm{erg\,g^{-1}}$. The stepsize was 5 s and the normal coefficient of restitution was set to 0.5. Although this image only shows one body (the largest), many smaller ones formed in a similar manner during the gravitational phase, such that at the end the size distribution consists mostly of aggregates, with a variety of spins and shapes, all produced by gravitational reaccumulation.

3.2. Rotational disruption

Fig. 3 is a comparison of the strength models (Section 2.5), showing the evolution of the cohesionless, rigid (non-deformable), and elastic cases, starting with a rapidly spinning aggregate. We start with aggregates spinning much faster than the cohesionless mass-loss limit in order to test the stress response, and to see whether mass loss results in binary formation (since YORP spin-up past the classical breakup limit for cohesionless bodies is now strongly suspected to play a role in the formation of near-Earth and small main belt asteroids; Walsh and Richardson, 2006b, 2008; Walsh et al., 2008). The result for the rigid case is typical: in over 300 simulations performed (of over 5000 particles each), starting from uniform random samplings of a parameter space of body axis ratio, fast initial spin, and a strength law of $S=kR^{-1/2}$ with two coefficient values (the extremes of $2.25\times10^{7}\,\mathrm{dyn\,cm^{-3/2}}$ and $2.25\times10^{8}\,\mathrm{dyn\,cm^{-3/2}}$ given in Holsapple, 2007, corresponding to the strength envelope that best fits

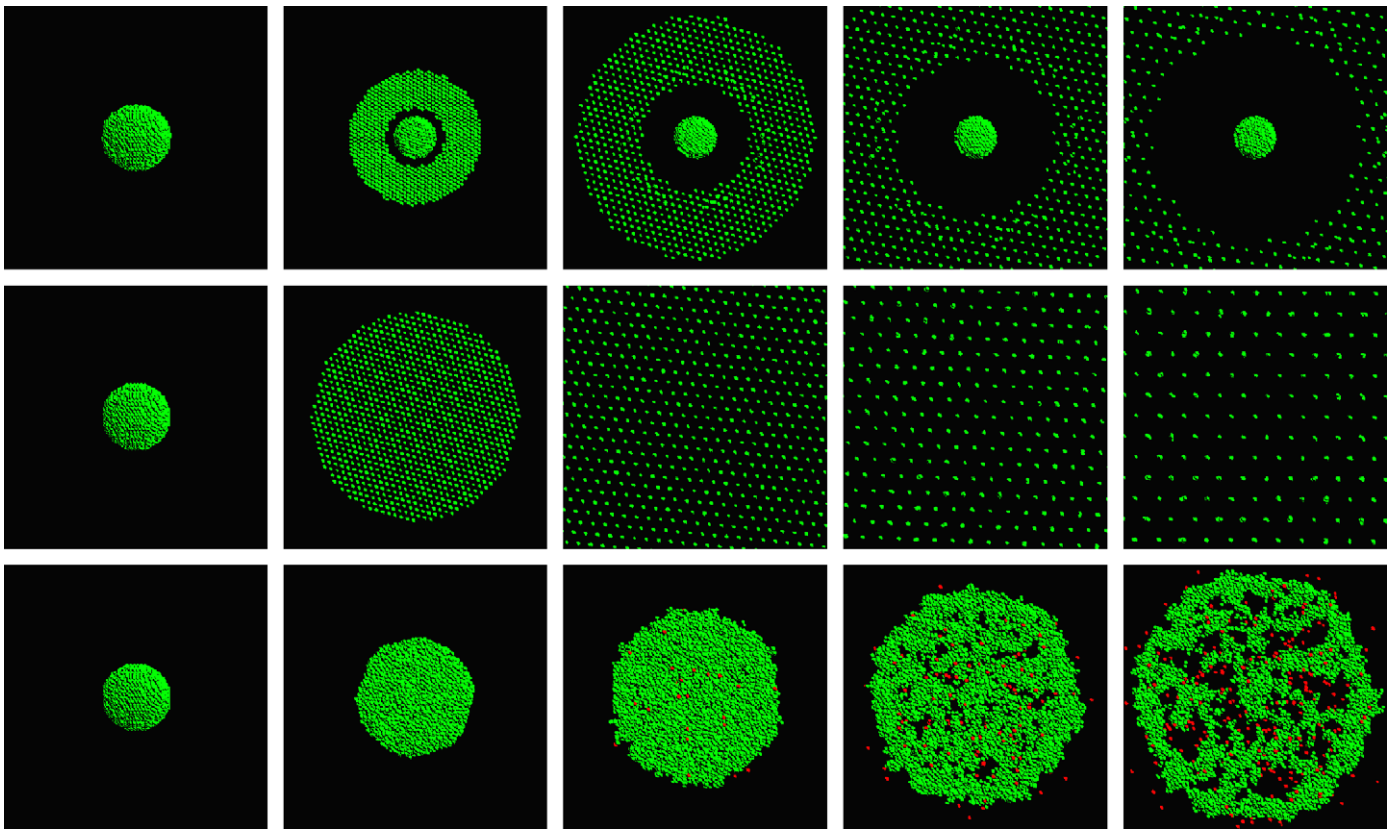

Fig. 3. Snapshots of the evolution of three strength cases: cohesionless (top row); rigid failure (middle); elastic failure (bottom). Evolution proceeds from left to right in each row; the snapshots are equally spaced in time. The initial condition was comparable in each case: an oblate aggregate spinning much faster than the cohesionless mass-loss spin limit (spin axis perpendicular to the page). In the elastic model, red particles have been permanently liberated. This particular case goes on to form a large, roughly spherical remnant with a sizable companion in a near-circular orbit.

observed asteroid spin data and extrapolation from laboratory experiment, respectively), not a single case resulted in satellite formation. Either the body survived without reshaping (because nowhere did the stress exceed the strength), or it lost an outer layer that escaped to infinity without any reaccumulation. The case of cohesionless bodies was explored in Richardson et al. (2005), but only for initially prolate shapes. Nonetheless, with a larger search space that included initially oblate shapes, we still find that no substantial amount of material remains in orbit around the remnant for any of the runs performed, but the remnant does typically reshape, with the most violent mass-loss cases leading to remnants that settle close to the Maclaurin/Jacobi fluid equilibrium configurations (also see Tanga et al., this issue).

The elastic case shown in Fig. 3, although not typical, illustrates a fairly common outcome in which failure proceeds by "fracturing" into strands, some of which later pull back together to form coherent clumps. In this particular case, a binary eventually forms. (The more typical outcome, when the initial spin greatly exceeds the cohesionless mass-loss spin limit, is for the body to fragment into tiny clumps that disperse to infinity.) For this model, a Young's modulus of 500 Pa was used, with a strength of 250 Pa. These values, though somewhat arbitrary, are comparable to upper limits derived for SL9 (Asphaug and Benz, 1996) and the Deep Impact target, Comet Tempel 1 (A'Hearn et al., 2005). The elastic model gives rise to binary formation in some cases because it allows deformation before failure. However, much work is needed to understand the applicability and limitations of this model.

4. Summary and future work

We have added the capability of modelling gravitational aggregates with strength to our simulation code `pkdgrav` by allowing spherical particles to bond together. The rigid body equations of motion with torque and off-axis dissipative collisions are solved during the regular integration step. Rules for collisional and rotational/tidal fragmentation are provided, with the latter enabled as either a rigid or elastic failure model. (The elastic failure model does not use the aggregate code.) We have begun exploring this vast new parameter space, concentrating on simulations of asteroid family formation and rotational disruption of asteroids. Current and future projects include simulations of rubble piles made up of small (two-, three-, four-particle) aggregates as a proxy for real, jumbled, irregular material, and implementing a wide array of strength models, including cases that allow plastic deformation (no restoring force).

Acknowledgments

This material is based upon work supported by the University of Maryland General Research Board, the National Aeronautics and Space Administration under Grant No. NAG511722 issued through the Office of Space Science, and by the National Science Foundation under Grant Nos. AST0307549 and AST0708110. Most simulations presented in this paper were carried out using computers in the Department of Astronomy at the University of Maryland, including the "borg" cluster administered by the Center for Theory and Computation, as well as the University of Maryland Office of Information Technology High Performance Computing Cluster. Some simulations were performed on the high performance computing facilities of the Mésocentre SIGAMM computer center of the Côte d'Azur Observatory, and we gratefully acknowledge both these facilities and the support of the staff, in particular A. and M.L. Miniussi. P.M. acknowledges support from the French Programme National de Planétologie. Raytracing for Figs. 1 and 2 was performed using the Persistence of Vision Raytracer.[2] The authors thank K. Holsapple and an anonymous reviewer for corrections and suggestions that improved the manuscript.

Appendix A. Collision prediction

A.1. Single particles

Consider two spherical particles of radius s_1 and s_2 on linear trajectories with relative speed $\mathbf{v} \equiv \mathbf{v}_2 - \mathbf{v}_1$ and initial relative position $\mathbf{r} \equiv \mathbf{r}_2 - \mathbf{r}_1$. We assume $r > s_1 + s_2$ (i.e., the particles are not overlapping or in contact). Suppose these particles are approaching one another (such that $\mathbf{r} \cdot \mathbf{v} < 0$) and collide at some future time t (such that their relative position vector $\mathbf{r}' \equiv \mathbf{r}'_2 - \mathbf{r}'_1$ has magnitude $r' = s_1 + s_2$). To solve for t, note that $\mathbf{r}' = \mathbf{v}t + \mathbf{r}$ for constant $\mathbf{v}$. Set $\mathbf{r}' \cdot \mathbf{r}' = (s_1 + s_2)^2$ (the condition for mutual contact), whence

$$v^2 t^2 + 2(\mathbf{r} \cdot \mathbf{v})t + r^2 = (s_1 + s_2)^2. \tag{A.1}$$

This is a quadratic equation with roots

$$t = \frac{-(\mathbf{r} \cdot \mathbf{v}) \pm \sqrt{(\mathbf{r} \cdot \mathbf{v})^2 - [r^2 - (s_1 + s_2)^2]v^2}}{v^2}, \tag{A.2}$$

where the smallest positive value of t is chosen to resolve the sign ambiguity.

A.2. Bonded aggregates

Now consider two aggregates, consisting of rigid collections of spheres, whose centers of mass are initially located at $\mathbf{R}_i$, $i = 1, 2$, and whose (constant) velocities are $\mathbf{V}_i$. Consider a spherical particle on each respective aggregate, located initially at position $\boldsymbol{\rho}_i$ in space coordinates with respect to each center of mass (so the initial space positions are $\mathbf{r}_i = \mathbf{R}_i + \boldsymbol{\rho}_i$). The velocity of each particle is a combination of the linear velocity of the aggregate plus the rotational motion about the aggregate center of mass. To second order, the space position of particle i after time t is given by

$$\mathbf{r}'_i = \left[\mathbf{V}_i + \boldsymbol{\Omega}_i \times \boldsymbol{\rho}_i + \tfrac{1}{2}\boldsymbol{\Omega}_i \times (\boldsymbol{\Omega}_i \times \boldsymbol{\rho}_i)t\right]t + \mathbf{r}_i, \tag{A.3}$$

where $\boldsymbol{\Omega}_i$ is the angular velocity of aggregate i (in the space frame), considered constant over a sufficiently small interval t. This expression was obtained by taking a Taylor expansion of the position vector to second order. Let $\mathbf{u}_i \equiv \mathbf{V}_i + \boldsymbol{\Omega}_\mathbf{i} \times \boldsymbol{\rho}_i$, $\mathbf{q}_i \equiv \boldsymbol{\Omega}_i \times (\boldsymbol{\Omega}_i \times \boldsymbol{\rho}_i)$, $\mathbf{u} \equiv \mathbf{u}_2 - \mathbf{u}_1$, and $\mathbf{q} \equiv \mathbf{q}_2 - \mathbf{q}_1$. Hence, $\mathbf{r}' = (\mathbf{u} + \frac{1}{2}\mathbf{q}t)t + \mathbf{r}$. Then, if as before we require $r' \equiv |\mathbf{r}'_2 - \mathbf{r}'_1| = s_1 + s_2$, we find

$$\tfrac{1}{4}q^2 t^4 + (\mathbf{u} \cdot \mathbf{q})t^3 + [u^2 + (\mathbf{r} \cdot \mathbf{q})]t^2 + 2(\mathbf{r} \cdot \mathbf{u})t + r^2 = (s_1 + s_2)^2, \tag{A.4}$$

This is a quartic equation in t for which the solution is non-trivial. For small t, the equation can be reduced to quadratic form by dropping the first two terms. The result is a good approximation for the time to contact between two spherical particles on two rotating aggregates:

$$t = \frac{-(\mathbf{r} \cdot \mathbf{u}) \pm \sqrt{(\mathbf{r} \cdot \mathbf{u})^2 - [r^2 - (s_1 + s_2)^2][u^2 + (\mathbf{r} \cdot \mathbf{q})]}}{u^2 + (\mathbf{r} \cdot \mathbf{q})} \tag{A.5}$$

(compare with Eq. (A.2)). Again the sign ambiguity is resolved by choosing the smallest positive t. For collisions between an aggregate and a single sphere, replace $\mathbf{u}_i$ with $\mathbf{v}_i$ and $\mathbf{q}_i$ with zero for the sphere in these expressions.

Appendix B. Collision resolution: non-central impacts

From the method of generalized coefficients (Brach, 1998), the change in velocity and spin of two aggregates made up of spheres involved in a point-contact collision is given by (cf. Richardson, 1995 for the derivation)

$$\begin{aligned}
\Delta\mathbf{V}_1 &= \gamma(1 + \varepsilon_n)(M_2/M)w_n\hat{\mathbf{n}},\\
\Delta\mathbf{V}_2 &= -\gamma(1 + \varepsilon_n)(M_1/M)w_n\hat{\mathbf{n}},\\
\Delta\boldsymbol{\Omega}_1 &= M_1\mathbf{I}_1^{-1}(\mathbf{c}_1 \times \Delta\mathbf{V}_1),\\
\Delta\boldsymbol{\Omega}_2 &= M_2\mathbf{I}_2^{-1}(\mathbf{c}_2 \times \Delta\mathbf{V}_2),
\end{aligned} \tag{B.1}$$

where M_i and $\mathbf{I}_i$ are the masses and inertia tensors of the aggregates ($M = M_1 + M_2$), ε_n is the normal coefficient of restitution, $\hat{\mathbf{n}}$ is a vector perpendicular to the contact plane and pointing toward body 2, $\mathbf{c}_i$ is a vector from aggregate i's center of mass to the contact point, $w_n = (\mathbf{w}_2 - \mathbf{w}_1) \cdot \hat{\mathbf{n}}$, $\mathbf{w}_i \equiv \mathbf{V}_i + \boldsymbol{\Omega}_i \times \mathbf{c}_i$, and γ is a factor that

[2] http://www.povray.org/

depends on the impact geometry:

$$\gamma^{-1} = 1 + \mu(a_{22}c_{1,p}^2 - 2a_{23}c_{1,t}c_{1,p} + a_{33}c_{1,t}^2 + b_{22}c_{2,p}^2 - 2b_{23}c_{2,t}c_{2,p} + b_{33}c_{2,t}^2), \quad \text{(B.2)}$$

where $\mu = M_1M_2/M$ is the reduced mass, t and p denote mutually perpendicular components tangential to the contact plane (constructed from $\hat{\mathbf{n}}$ by the Gram–Schmidt orthonormalization process), and $\mathbf{a} = (a_{kk})$ and $\mathbf{b} = (b_{kk})$ are the inverses of the inertia tensors of the aggregates, expressed in this new *ntp* coordinate system. The latter matrices are obtained by noting that

$$\mathbf{I}_{ntp} = \mathbf{X}^{\mathrm{T}}\mathbf{I}\mathbf{X}, \quad \text{(B.3)}$$

where $\mathbf{I}$ is the inertia tensor in the space frame and $\mathbf{X} = (\hat{\mathbf{n}}|\hat{\mathbf{t}}|\hat{\mathbf{p}})$ is a matrix whose columns are the basis vectors of the *ntp* coordinate system.

For collisions between an aggregate and a single sphere, replace $\mathbf{c}_i$ with $(3-2i)R_i\hat{\mathbf{n}}$, where R_i is the radius of the sphere in question ($i = 1, 2$), so $c_{i,t} = 0 = c_{i,p}$. If both colliders are single spheres, the system reduces to the familiar billiard-ball equations without surface friction ($\gamma = 1$, $\Delta\boldsymbol{\Omega}_1 = 0 = \Delta\boldsymbol{\Omega}_2$, and w_n becomes just the normal component of the relative velocity). Surface friction greatly increases the complexity of the restitution equations for non-central impacts and may not lead to unique solutions (see Brach, 1998 for details); therefore, surface friction is not implemented in `pkdgrav` for non-spherical rigid bodies.

References

A'Hearn, M.F., et al., 2005. Deep impact: excavating Comet Tempel 1. Science 310, 258–264.

Anderson, J.D., Anabtawi, A., Jacobson, R.A., Johnson, T.V., Lau, E.L., Moore, W.B., Schubert, G., Taylor, A.H., Thomas, P.C., Weinwurm, G., 2002. Gravity field, topography, and interior structure of Amalthea. In: Fall 2002 AGU, P12C-13, pp. 3–4.

Asphaug, E., Benz, W., 1994. Density of Comet Shoemaker-Levy 9 deduced by modelling breakup of the parent "rubble pile". Nature 370, 120–124.

Asphaug, E., Benz, W., 1996. Size, density, and structure of Comet Shoemaker-Levy 9 inferred from the physics of tidal breakup. Icarus 121, 225–248.

Asphaug, E., Melosh, H.J., 1993. The Stickney impact of Phobos: a dynamical model. Icarus 101, 144–164.

Asphaug, E., Ostro, S.J., Hudson, R.S., Scheeres, D.J., Benz, W., 1998. Disruption of kilometre-sized asteroids by energetic collisions. Nature 393, 437–440.

Barnes, J., Hut, P., 1986. A hierarchical $\mathcal{O}(N \log N)$ force-calculation algorithm. Nature 324, 446–449.

Bottke Jr., W.F., Melosh, H.J., 1996a. Formation of asteroid satellites and doublet craters by planetary tidal forces. Nature 381, 51–53.

Bottke Jr., W.F., Melosh, H.J., 1996b. Binary asteroids and the formation of doublet craters. Icarus 124, 372–391.

Bottke Jr., W.F., Richardson, D.C., Love, S.G., 1997. Can tidal disruption of asteroids make crater chains on the Earth and Moon? Icarus 126, 470–474.

Bottke Jr., W.F., Richardson, D.C., Michel, P., Love, S.G., 1999. 1620 Geographos and 433 Eros: shaped by planetary tides? Astron. J. 177, 1921–1928.

Bottke Jr., W.F., Vokrouhlický, D., Rubincam, D.P., Brož, M., 2002. The effect of Yarkovsky thermal forces on the dynamical evolution of asteroids and meteoroids. In: Bottke Jr., W.F., Cellino, A., Paolicchi, P., Binzel, R.P. (Eds.), Asteroids III. University of Arizona Press, Tucson, pp. 395–408.

Bottke Jr., W.F., Vokrouhlický, D., Rubincam, D.P., Nesvorný, D., 2006. The Yarkovsky and YORP effects: implications for asteroid dynamics. Annu. Rev. Earth Planet. Sci. 34, 157–191.

Brach, R.M., 1998. Formulation of rigid body impact problems using generalized coefficients. Int. J. Eng. Sci. 36, 61–71.

Durda, D.D., Bottke Jr., W.F., Enke, B.L., Merline, W.J., Asphaug, E., Richardson, D.C., Leinhardt, Z.M., 2004. The formation of asteroid satellites in large impacts: results from numerical simulations. Icarus 167, 382–396 (Also see Erratum, Icarus 170, 242, and reprinted article, Icarus 170, 243–257.).

Durda, D.D., Bottke Jr., W.F., Nesvorný, D., Enke, B.L., Merline, W.J., Asphaug, A., Richardson, D.C., 2007. Size–frequency distributions of fragments from SPH/N-body simulations of asteroid impacts: comparison with observed asteroid families. Icarus 186, 498–516.

Farnham, T.L., Schleicher, D.G., Woodney, L.M., Birch, P.V., Eberhardy, C.A., Levy, L., 2001. Imaging and photometry of Comet C/1999 S4 (LINEAR) before perihelion and after breakup. Science 292, 1348–1354.

Fujiwara, A., et al., 2006. The rubble-pile asteroid Itokawa as observed by Hayabusa. Science 312, 1330–1334.

Holsapple, K.A., 2007. Spin limits of solar system bodies: from the small fast-rotators to 2003 EL61. Icarus 187, 500–509.

Housen, K.R., Holsapple, K.A., 2003. Impact cratering on porous asteroids. Icarus 163, 102–119.

Housen, K.R., Holsapple, K.A., Voss, M.E., 1999. Compaction as the origin of the unusual craters on the asteroid Mathilde. Nature 402, 155–157.

Korycansky, D.G., Asphaug, E., 2006. Low-speed impacts between rubble piles modeled as collections of polyhedra. Icarus 181, 605–617.

Love, S.G., Ahrens, T.J., 1996. Catastrophic impacts on gravity dominated asteroids. Icarus 124, 141–155.

Merline, W.J., Close, L.M., Dumas, C., Chapman, C.R., Roddier, F., Ménard, F., Slater, D.C., Duvert, G., Shelton, C., Morgan, T., 1999. Discovery of a moon orbiting the asteroid 45 Eugenia. Nature 401, 565–568.

Michel, P., Benz, W., Tanga, P., Richardson, D.C., 2001. Collisions and gravitational reaccumulation: forming asteroid families and satellites. Science 294, 1696–1700.

Michel, P., Tanga, P., Benz, W., Richardson, D.C., 2002. Formation of asteroid families by catastrophic disruption: simulations with fragmentation and gravitational re-accumulation. Icarus 160, 10–23.

Michel, P., Benz, W., Richardson, D.C., 2003. Disruption of fragmented parent bodies as the origin of asteroid families. Nature 421, 608–611.

Michel, P., Benz, W., Richardson, D.C., 2004a. Catastrophic disruption of pre-shattered parent bodies. Icarus 168, 420–432.

Michel, P., Benz, W., Richardson, D.C., 2004b. Catastrophic disruption of asteroids and family formation: a review of numerical simulations including both fragmentation and gravitational reaccumulations. Planet Space Sci. 52, 1109–1117.

Michel, P., Richardson, D.C., Benz, W., 2008. On the shape, spin, size, and mass of gravitational aggregates in simulations of asteroid family formation. Icarus, in preparation.

Ostro, S.J., et al., 1995. Extreme elongation of asteroid 1620 Geographos from radar images. Nature 375, 474–477.

Pravec, P., Harris, A.W., 2000. Fast and slow rotation of asteroids. Icarus 148, 12–20.

Pravec, P., Harris, A.W., Michalowski, T., 2002. Asteroid rotations. In: Bottke Jr., W.F., Cellino, A., Paolicchi, P., Binzel, R.P. (Eds.), Asteroids III. University of Arizona Press, Tucson, pp. 113–122.

Pravec, P., et al., 2005. Photometric survey of binary near-Earth asteroids. Icarus 181, 63–93.

Richardson, D.C., 1994. Tree code simulations of planetary rings. Mon. Not. R. Astron. Soc. 269, 493–511.

Richardson, D.C., 1995. A self-consistent numerical treatment of fractal aggregate dynamics. Icarus 115, 320–335.

Richardson, D.C., Walsh, K.J., 2006. Binary minor planets. Annu. Rev. Earth Planet. Sci. 34, 47–81.

Richardson, D.C., Bottke Jr., W.F., Love, S.G., 1998. Tidal distortion and disruption of Earth-crossing asteroids. Icarus 134, 47–76.

Richardson, D.C., Quinn, T., Stadel, J., Lake, G., 2000. Direct large-scale *N*-body simulations of planetesimal dynamics. Icarus 143, 45–59.

Richardson, D.C., Leinhardt, Z.M., Melosh, H.J., Bottke Jr., W.F., Asphaug, E., 2002. Gravitational aggregates: evidence and evolution. In: Bottke Jr., W.F., Cellino, A., Paolicchi, P., Binzel, R.P. (Eds.), Asteroids III. University of Arizona Press, Tucson, pp. 501–515.

Richardson, D.C., Elankumaran, P., Sanderson, R.E., 2005. Numerical experiments with rubble piles: equilibrium shapes and spins. Icarus 173, 349–361.

Roig, F., Duffard, R., Penteado, P., Lazzaro, D., Kodama, T., 2003. Interacting ellipsoids: a minimal model for the dynamics of rubble-pile bodies. Icarus 165, 355–370.

Rubincam, D.P., 2000. Radiative spin-up and spin-down of small asteroids. Icarus 148, 2–11.

Saha, P., Tremaine, S., 1992. Symplectic integrators for solar system dynamics. Astron. J. 104, 1633–1640.

Schenk, P.M., Asphaug, E., McKinnon, W.B., Melosh, H.J., Weissman, P.R., 1996. Cometary nuclei and tidal disruption: the geological record of crater chains on Callisto and Ganymede. Icarus 121, 249–274.

Stadel, J., 2001. Cosmological *N*-body simulations and their analysis. Thesis, University of Washington, Seattle, 126pp.

Tanga, P., Hestroffer, D., Delbò, M., Richardson, D.C., 2008. Asteroid rotation and shape from disruption to gravitational reaccumulation. Planet Space Sci., this issue, doi:10.1016/j.pss.2008.06.016.

Veverka, J., et al., 1997. NEAR's flyby of 253 Mathilde: images of a C asteroid. Science 278, 2109–2114.

Vokrouhlický, D., Capek, D., 2002. YORP-induced long-term evolution of the spin state of small asteroids and meteoroids: Rubincam's approximation. Icarus 159, 449–467.

Walsh, K.J., Richardson, D.C., 2006a. Binary near-Earth asteroid formation: rubble pile model of tidal disruptions. Icarus 180, 201–216.

Walsh, K.J., Richardson, D.C., 2006b. Steady-state population of the NEA binaries and YORP spinup models. Bull. Am. Astr. Soc. 38, #53.08.

Walsh, K.J., Richardson, D.C., 2008. A steady-state model of NEA binaries formed by tidal disruption of gravitational aggregates. Icarus 193, 553–566.

Walsh, K.J., Richardson, D.C., Rettig, T.W., 2003. Modeling the breakup of Comet Shoemaker-Levy 9. Astron. Soc. Pacific Conf. Ser. 291, 415.

Walsh, K.J., Richardson, D.C., Michel, P., 2008. Rotational breakup as the origin of small binary asteroids. Nature, in press, doi:10.1038/nature07078.

Yeomans, D.K., et al., 1997. Estimating the mass of asteroid 253 Mathilde from tracking data during the NEAR flyby. Science 278, 2106–2109.